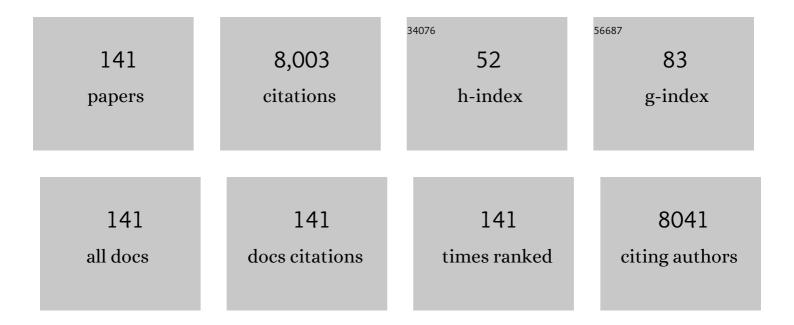
Hongzhi Cui

List of Publications by Year in descending order

Source: https://exaly.com/author-pdf/3454533/publications.pdf Version: 2024-02-01



#	Article	IF	CITATIONS
1	2D/2D/2D heterojunction of Ti3C2 MXene/MoS2 nanosheets/TiO2 nanosheets with exposed (001) facets toward enhanced photocatalytic hydrogen production activity. Applied Catalysis B: Environmental, 2019, 246, 12-20.	10.8	373
2	3D Bi ₂ MoO ₆ Nanosheet/TiO ₂ Nanobelt Heterostructure: Enhanced Photocatalytic Activities and Photoelectochemistry Performance. ACS Catalysis, 2015, 5, 4530-4536.	5.5	323
3	Boosting the Photocatalytic Ability of g-C ₃ N ₄ for Hydrogen Production by Ti ₃ C ₂ MXene Quantum Dots. ACS Applied Materials & Interfaces, 2019, 11, 41440-41447.	4.0	289
4	Ti3C2 MXene-derived Ti3C2/TiO2 nanoflowers for noble-metal-free photocatalytic overall water splitting. Applied Materials Today, 2018, 13, 217-227.	2.3	250
5	High Detectivity and Rapid Response in Perovskite CsPbBr ₃ Single-Crystal Photodetector. Journal of Physical Chemistry C, 2017, 121, 4917-4923.	1.5	241
6	Ag 2 O nanoparticle/TiO 2 nanobelt heterostructures with remarkable photo-response and photocatalytic properties under UV, visible and near-infrared irradiation. Applied Catalysis B: Environmental, 2016, 198, 83-90.	10.8	219
7	The selective deposition of MoS2 nanosheets onto (101) facets of TiO2 nanosheets with exposed (001) facets and their enhanced photocatalytic H2 production. Applied Catalysis B: Environmental, 2019, 241, 329-337.	10.8	198
8	The fabrication of 1D/2D CdS nanorod@Ti3C2 MXene composites for good photocatalytic activity of hydrogen generation and ammonia synthesis. Chemical Engineering Journal, 2021, 406, 127177.	6.6	187
9	Synergetic effect of defects rich MoS2 and Ti3C2 MXene as cocatalysts for enhanced photocatalytic H2 production activity of TiO2. Chemical Engineering Journal, 2020, 383, 123178.	6.6	175
10	Single-Atom Pt–N ₃ Sites on the Stable Covalent Triazine Framework Nanosheets for Photocatalytic N ₂ Fixation. ACS Catalysis, 2020, 10, 2431-2442.	5.5	171
11	Photocatalytic H2 Evolution on TiO2 Assembled with Ti3C2 MXene and Metallic 1T-WS2 as Co-catalysts. Nano-Micro Letters, 2020, 12, 6.	14.4	141
12	Controllable growth of MoS2 nanosheets on novel Cu2S snowflakes with high photocatalytic activity. Applied Catalysis B: Environmental, 2018, 232, 355-364.	10.8	129
13	Co doped MoS2 as cocatalyst considerably improved photocatalytic hydrogen evolution of g-C3N4 in an alkalescent environment. Chemical Engineering Journal, 2021, 421, 130016.	6.6	127
14	Porous g-C3N4 with nitrogen defects and cyano groups for excellent photocatalytic nitrogen fixation without co-catalysts. Journal of Colloid and Interface Science, 2019, 556, 206-213.	5.0	125
15	Full solar spectrum photocatalytic oxygen evolution by carbon-coated TiO2 hierarchical nanotubes. Applied Catalysis B: Environmental, 2019, 243, 711-720.	10.8	117
16	The metallic 1T-phase WS2 nanosheets as cocatalysts for enhancing the photocatalytic hydrogen evolution of g-C3N4 nanotubes. Applied Catalysis B: Environmental, 2020, 274, 119114.	10.8	116
17	Highly efficient full solar spectrum (UV-vis-NIR) photocatalytic performance of Ag2S quantum dot/TiO2 nanobelt heterostructures. Journal of Industrial and Engineering Chemistry, 2017, 45, 189-196.	2.9	103
18	Porous ZnO Ultrathin Nanosheets with High Specific Surface Areas and Abundant Oxygen Vacancies for Acetylacetone Gas Sensing. ACS Applied Materials & Interfaces, 2019, 11, 24757-24763.	4.0	100

#	Article	IF	CITATIONS
19	Silver oxide decorated graphitic carbon nitride for the realization of photocatalytic degradation over the full solar spectrum: From UV to NIR region. Solar Energy Materials and Solar Cells, 2017, 168, 100-111.	3.0	99
20	Bi ₂ WO ₆ Nanosheets Decorated with Au Nanorods for Enhanced Nearâ€Infrared Photocatalytic Properties Based on Surface Plasmon Resonance Effects and Wideâ€Range Nearâ€Infrared Light Harvesting. ChemCatChem, 2017, 9, 1511-1516.	1.8	95
21	A novel high-entropy alloy composite coating with core-shell structures prepared by plasma cladding. Vacuum, 2021, 184, 109905.	1.6	94
22	Two-dimensional/one-dimensional molybdenum sulfide (MoS2) nanoflake/graphitic carbon nitride (g-C3N4) hollow nanotube photocatalyst for enhanced photocatalytic hydrogen production activity. Journal of Colloid and Interface Science, 2020, 567, 300-307.	5.0	93
23	High-Performance Electrocatalytic Conversion of N ₂ to NH ₃ Using 1T-MoS ₂ Anchored on Ti ₃ C ₂ MXene under Ambient Conditions. ACS Applied Materials & Interfaces, 2020, 12, 26060-26067.	4.0	92
24	Fabrication of 1D Zn2SnO4 nanowire and 2D ZnO nanosheet hybrid hierarchical structures for use in triethylamine gas sensors. Sensors and Actuators B: Chemical, 2019, 291, 155-163.	4.0	91
25	Hydrogenated TiO2 nanobelts as highly efficient photocatalytic organic dye degradation and hydrogen evolution photocatalyst. Journal of Hazardous Materials, 2015, 299, 165-173.	6.5	89
26	Synthesis of few-layer MoS2 nanosheets-coated TiO2 nanosheets on graphite fibers for enhanced photocatalytic properties. Solar Energy Materials and Solar Cells, 2017, 172, 108-116.	3.0	89
27	High response and selectivity of single crystalline ZnO nanorods modified by In2O3 nanoparticles for n-butanol gas sensing. Sensors and Actuators B: Chemical, 2018, 277, 144-151.	4.0	88
28	Enhanced Optoelectronic Performance on the (110) Lattice Plane of an MAPbBr ₃ Single Crystal. Journal of Physical Chemistry Letters, 2017, 8, 684-689.	2.1	82
29	Effects of Ti-to-Al ratios on the phases, microstructures, mechanical properties, and corrosion resistance of Al2-xCoCrFeNiTix high-entropy alloys. Journal of Alloys and Compounds, 2019, 805, 585-596.	2.8	81
30	1T-MoS ₂ nanopatch/Ti ₃ C ₂ MXene/TiO ₂ nanosheet hybrids for efficient photocatalytic hydrogen evolution. Materials Chemistry Frontiers, 2019, 3, 2673-2680.	3.2	81
31	Phosphorous-doped 1T-MoS2 decorated nitrogen-doped g-C3N4 nanosheets for enhanced photocatalytic nitrogen fixation. Journal of Colloid and Interface Science, 2022, 605, 320-329.	5.0	81
32	Hierarchical assembly of In 2 O 3 nanoparticles on ZnO hollow nanotubes using carbon fibers as templates: Enhanced photocatalytic and gas-sensing properties. Journal of Colloid and Interface Science, 2017, 498, 263-270.	5.0	78
33	Facile synthesis of heterojunction of MXenes/TiO2 nanoparticles towards enhanced hexavalent chromium removal. Journal of Colloid and Interface Science, 2020, 561, 46-57.	5.0	78
34	Towards full-spectrum (UV, visible, and near-infrared) photocatalysis: achieving an all-solid-state Z-scheme between Ag ₂ O and TiO ₂ using reduced graphene oxide as the electron mediator. Catalysis Science and Technology, 2017, 7, 4193-4205.	2.1	76
35	Metallic 1T-phase MoS ₂ quantum dots/g-C ₃ N ₄ heterojunctions for enhanced photocatalytic hydrogen evolution. Nanoscale, 2019, 11, 12266-12274.	2.8	76
36	Linking growth mode to lengths of single-walled carbon nanotubes. Carbon, 2017, 113, 231-236.	5.4	75

#	Article	IF	CITATIONS
37	Rationalizing and controlling the phase transformation of semi-metallic 1T′-phase and semi-conductive 2H-phase MoS2 as cocatalysts for photocatalytic hydrogen evolution. Chemical Engineering Journal, 2020, 396, 125344.	6.6	71
38	Wear and corrosion properties of B4C-added CoCrNiMo high-entropy alloy coatings with in-situ coherent ceramic. Materials and Design, 2021, 210, 110068.	3.3	71
39	High yield production of reduced TiO2 with enhanced photocatalytic activity. Applied Surface Science, 2016, 360, 738-743.	3.1	70
40	Synthesis of novel Ag/Ag2O heterostructures with solar full spectrum (UV, visible and near-infrared) light-driven photocatalytic activity and enhanced photoelectrochemical performance. Catalysis Communications, 2016, 87, 82-85.	1.6	68
41	1â€⊤-phase molybdenum sulfide nanodots enable efficient electrocatalytic nitrogen fixation under ambient conditions. Applied Catalysis B: Environmental, 2020, 272, 118984.	10.8	68
42	Facile preparation of metallic 1T phase molybdenum selenide as cocatalyst coupled with graphitic carbon nitride for enhanced photocatalytic H2 production. Journal of Colloid and Interface Science, 2021, 598, 172-180.	5.0	68
43	Interfacial Microstructure and Enhanced Mechanical Properties of Carbon Fiber Composites Caused by Growing Generation 1–4 Dendritic Poly(amidoamine) on a Fiber Surface. Langmuir, 2016, 32, 8339-8349.	1.6	67
44	Gold nanorods/g-C3N4 heterostructures for plasmon-enhanced photocatalytic H2 evolution in visible and near-infrared light. Journal of Colloid and Interface Science, 2019, 557, 700-708.	5.0	66
45	A simple strategy for fabrication of an FCC-based complex concentrated alloy coating with hierarchical nanoprecipitates and enhanced mechanical properties. Materials and Design, 2019, 180, 107893.	3.3	66
46	Construction of hierarchical 2D/2D Ti3C2/MoS2 nanocomposites for high-efficiency solar steam generation. Journal of Colloid and Interface Science, 2021, 584, 125-133.	5.0	66
47	Design Growth of MAPbI ₃ Single Crystal with (220) Facets Exposed and Its Superior Optoelectronic Properties. Journal of Physical Chemistry Letters, 2018, 9, 216-221.	2.1	64
48	Core-double shell ZnO@In2O3@ZnO hollow microspheres for superior ethanol gas sensing. Sensors and Actuators B: Chemical, 2021, 341, 130002.	4.0	62
49	High-quality inorganic–organic perovskite CH3NH3PbI3 single crystals for photo-detector applications. Journal of Materials Science, 2017, 52, 276-284.	1.7	61
50	Oxygen vacancy-rich BiO2-x ultra-thin nanosheet for efficient full-spectrum responsive photocatalytic oxygen evolution from water splitting. Solar Energy Materials and Solar Cells, 2019, 195, 309-317.	3.0	60
51	Visible photocatalytic and photoelectrochemical activities of TiO2 nanobelts modified by In2O3 nanoparticles. Journal of Colloid and Interface Science, 2017, 487, 258-265.	5.0	58
52	Effect of carbon reactant on microstructures and mechanical properties of TiAl/Ti 2 AlC composites. Materials Science & Engineering A: Structural Materials: Properties, Microstructure and Processing, 2017, 684, 406-412.	2.6	56
53	RuO2/TiO2 nanobelt heterostructures with enhanced photocatalytic activity and gas-phase selective oxidation of benzyl alcohol. Solar Energy Materials and Solar Cells, 2016, 151, 7-13.	3.0	55
54	A New Design of In Situ Ti(C,N) Reinforced Composite Coatings and Their Microstructures, Interfaces, and Wear Resistances. ACS Applied Materials & Interfaces, 2018, 10, 4250-4265.	4.0	54

#	Article	IF	CITATIONS
55	Titanium carbide MXenes coupled with cadmium sulfide nanosheets as two-dimensional/two-dimensional heterostructures for photocatalytic hydrogen production. Journal of Colloid and Interface Science, 2022, 613, 644-651.	5.0	53
56	TiO2 nanobelts with anatase/rutile heterophase junctions for highly efficient photocatalytic overall water splitting. Journal of Colloid and Interface Science, 2020, 567, 181-189.	5.0	52
57	Novel Ag2O nanoparticles modified MoS2 nanoflowers for piezoelectric-assisted full solar spectrum photocatalysis. Journal of Colloid and Interface Science, 2019, 537, 206-214.	5.0	50
58	Controlled growth of MAPbBr3 single crystal: understanding the growth morphologies of vicinal hillocks on (100) facet to form perfect cubes. Journal of Materials Science, 2017, 52, 7907-7916.	1.7	48
59	Large-scale synthesis of porous nickel boride for robust hydrogen evolution reaction electrocatalyst. Applied Surface Science, 2019, 470, 591-595.	3.1	48
60	1T-phase MoS ₂ quantum dots as a superior co-catalyst to Pt decorated on carbon nitride nanorods for photocatalytic hydrogen evolution from water. Materials Chemistry Frontiers, 2019, 3, 2032-2040.	3.2	45
61	Growth of porous ZnO single crystal hierarchical architectures with ultrahigh sensing performances to ethanol and acetone gases. Ceramics International, 2017, 43, 1121-1128.	2.3	44
62	Growth kinetics of single-walled carbon nanotubes with a (2 <i>n</i> , <i>n</i>) chirality selection. Science Advances, 2019, 5, eaav9668.	4.7	42
63	Adsorption and intercalation of organic pollutants and heavy metal ions into MgAl-LDHs nanosheets with high capacity. RSC Advances, 2016, 6, 92402-92410.	1.7	41
64	Bi ₂ O ₃ nanoparticles incorporated porous TiO ₂ films as an effective <i>p</i> â€ <i>n</i> junction with enhanced photocatalytic activity. Journal of the American Ceramic Society, 2017, 100, 1339-1349.	1.9	41
65	Enhanced strength and ductility in a spark plasma sintered CoCrCuO·5NiAl0.5 high-entropy alloy via a double-step ball milling approach for processing powders. Materials Science & Engineering A: Structural Materials: Properties, Microstructure and Processing, 2019, 762, 138071.	2.6	39
66	Integrating the Z-scheme heterojunction into a novel Ag2O@rGO@reduced TiO2 photocatalyst: Broadened light absorption and accelerated charge separation co-mediated highly efficient UV/visible/NIR light photocatalysis. Journal of Colloid and Interface Science, 2019, 538, 689-698.	5.0	39
67	Synthesis of salicylic acid-modified graphite carbon nitride for enhancing photocatalytic nitrogen fixation. Journal of Colloid and Interface Science, 2020, 571, 318-325.	5.0	38
68	In ₂ O ₃ Nanoparticles Decorated ZnO Hierarchical Structures for <i>n</i> Butanol Sensor. ACS Applied Nano Materials, 2020, 3, 3295-3304.	2.4	37
69	TiO ₂ Nanobelts Decorated with In ₂ S ₃ Nanoparticles as Photocatalysts with Enhanced Fullâ€6olarâ€6pectrum (UV–vis–NIR) Photocatalytic Activity toward the Degradation of Tetracycline. Particle and Particle Systems Characterization, 2017, 34, 1700127.	1.2	36
70	Scalable and low-cost fabrication of hydrophobic PVDF/WS2 porous membrane for highly efficient solar steam generation. Journal of Colloid and Interface Science, 2021, 588, 369-377.	5.0	36
71	Synthesis of In ₂ O ₃ nanoparticle/TiO ₂ nanobelt heterostructures for near room temperature ethanol sensing. RSC Advances, 2017, 7, 11503-11509.	1.7	35
72	Vanadium sulfide sub-microspheres: A new near-infrared-driven photocatalyst. Journal of Colloid and Interface Science, 2017, 498, 442-448.	5.0	35

#	Article	IF	CITATIONS
73	The microstructures and properties changes induced by Al:Co ratios of the Al CrCo FeNi high entropy alloys. Materials Science & Engineering A: Structural Materials: Properties, Microstructure and Processing, 2018, 733, 153-163.	2.6	34
74	Fabrication of TiO2 nanoflowers with bronze (TiO2(B))/anatase heterophase junctions for efficient photocatalytic hydrogen production. International Journal of Hydrogen Energy, 2019, 44, 24398-24406.	3.8	34
75	SnO2 core-shell hollow microspheres co-modification with Au and NiO nanoparticles for acetone gas sensing. Powder Technology, 2020, 364, 159-166.	2.1	34
76	The metallic 1T-WS2 as cocatalysts for promoting photocatalytic N2 fixation performance of Bi5O7Br nanosheets. Chinese Chemical Letters, 2021, 32, 3501-3504.	4.8	32
77	Self-assembled silane film and silver nanoparticles coating on magnesium alloys for corrosion resistance and antibacterial applications. Acta Metallurgica Sinica (English Letters), 2013, 26, 681-686.	1.5	31
78	Anisotropic optoelectronic performances on (112) and (100) lattice plane of perovskite MAPbI3 single crystal. Materials Chemistry and Physics, 2018, 204, 222-227.	2.0	31
79	Effect of plasma remelting on microstructure and properties of a CoCrCuNiAl0.5 high-entropy alloy prepared by spark plasma sintering. Journal of Materials Science, 2021, 56, 5878-5898.	1.7	31
80	Cesium Decreases Defect Density and Enhances Optoelectronic Properties of Mixed MA _{1–<i>x</i>} Cs <i>_x</i> PbBr ₃ Single Crystal. Journal of Physical Chemistry C, 2019, 123, 14969-14975.	1.5	30
81	Ni/Co/black phosphorus nanocomposites for Q235 carbon steel corrosion-resistant coating. Advanced Composites and Hybrid Materials, 2022, 5, 438-449.	9.9	30
82	Ru nanoparticles decorated TiO 2 nanobelts: A heterostructure towards enhanced photocatalytic activity and gas-phase selective oxidation of benzyl alcohol. Ceramics International, 2016, 42, 1611-1617.	2.3	29
83	Highly efficient photocatalytic activity of Ag ₃ PO ₄ /Ag/ZnS(en) _{0.5} photocatalysts through Z-scheme photocatalytic mechanism. RSC Advances, 2017, 7, 18392-18399.	1.7	29
84	Fabrication of Au decorated porous ZnO microspheres with enhanced gas sensing properties. Powder Technology, 2017, 315, 379-384.	2.1	28
85	Controllable 3D interconnected featured pore structure of transition metal borides-carbonitride/MoS2 for efficiently solar evaporation and wastewater purification. Chemical Engineering Journal, 2022, 446, 137275.	6.6	28
86	Noble metal-like behavior of plasmonic Bi particles deposited on reduced TiO2 microspheres for efficient full solar spectrum photocatalytic oxygen evolution. Chinese Journal of Catalysis, 2020, 41, 333-340.	6.9	27
87	Preparation of mesoporous SnO 2 by solvothermal method using Stahlianthus involucratus leaves and application to n-butanol sensor. Powder Technology, 2016, 302, 283-287.	2.1	26
88	Facile synthesis and superior ethyl acetate sensing performance of Au decorated ZnO flower-like architectures. Ceramics International, 2017, 43, 5053-5060.	2.3	26
89	Solvothermal preparation and gas sensing properties of hierarchical pore structure SnO 2 produced using grapefruit peel as a bio-template. Ceramics International, 2017, 43, 4112-4118.	2.3	25
90	Preparation of porous Al2TiO5-Mullite ceramic by starch consolidation casting and its corrosion resistance characterization. Ceramics International, 2016, 42, 14107-14112.	2.3	24

Номсин Си

#	Article	IF	CITATIONS
91	Synergistic improvement of wear and corrosion resistance of CoCrNiMoCB coatings obtained by laser cladding: Role of Mo concentration. Materials and Design, 2022, 219, 110751.	3.3	24
92	Preparation of porous Al2TiO5 ceramics reinforced by in situ formation of mullite whiskers. Materials & Design, 2013, 47, 57-60.	5.1	23
93	High temperature growth of single-walled carbon nanotubes with a narrow chirality distribution by tip-growth mode. Chemical Engineering Journal, 2018, 341, 344-350.	6.6	23
94	Ti ₂ Al(C, N) Solid Solution Reinforcing TiAl-Based Composites: Evolution of a Core–Shell Structure, Interfaces, and Mechanical Properties. ACS Applied Materials & Interfaces, 2018, 10, 16783-16792.	4.0	22
95	Synthesis of porous few-layer carbon nitride with excellent photocatalytic nitrogen fixation. Journal of Materiomics, 2020, 6, 128-137.	2.8	22
96	Addition Al and/or Ti Induced Modifications of Microstructures, Mechanical Properties, and Corrosion Properties in CoCrFeNi High-Entropy Alloy Coatings. Acta Metallurgica Sinica (English) Tj ETQq0 0 0 rg	BT1/Øverlo	ock2120 Tf 50 5
97	Porous graphitic carbon nitride with nitrogen defects and cobalt-nitrogen (Co N) bonds for efficient broad spectrum (visible and near-infrared) photocatalytic H2 production. Journal of Colloid and Interface Science, 2020, 561, 719-729.	5.0	21
98	Facile synthesis of mesoporous SnO2 microspheres using bioactive yeast cell. Powder Technology, 2016, 301, 96-101.	2.1	20
99	The high surface energy of NiO {110} facets incorporated into TiO2 hollow microspheres by etching Ti plate for enhanced photocatalytic and photoelectrochemical activity. Applied Surface Science, 2017, 396, 1539-1545.	3.1	20
100	Fabrication of molybdenum and tungsten oxide, sulfide, phosphide (MoxW1-xO2/MoxW1-xS2/MoxW1-xP) porous hollow nano-octahedrons from metal-organic frameworks templates as efficient hydrogen evolution reaction electrocatalysts. Journal of Colloid and Interface Science, 2019, 547, 339-349.	5.0	20
101	Non-high temperature method to synthesize carbon coated TiO2 nano-dendrites for enhanced wide spectrum photocatalytic hydrogen evolution activity. Journal of Colloid and Interface Science, 2020, 571, 412-418.	5.0	20
102	Incorporation of Cesium Ions into MA _{1–<i>x</i>} Cs _{<i>x</i>} PbI ₃ Single Crystals: Crystal Growth, Enhancement of Stability, and Optoelectronic Properties. Journal of Physical Chemistry Letters, 2018, 9, 5833-5839.	2.1	19
103	Remarkable charge separation and photocatalytic efficiency enhancement through TiO2(B)/anatase hetrophase junctions of TiO2 nanobelts. International Journal of Hydrogen Energy, 2019, 44, 27311-27318.	3.8	19
104	Formation and beneficial effects of the amorphous/nanocrystalline phase in laser remelted (FeCoCrNi)75Nb10B8Si7 high-entropy alloy coatings fabricated by plasma cladding. Journal of Alloys and Compounds, 2022, 899, 163277.	2.8	18
105	Three-Dimensional Artificial Transpiration Structure Based on 1T/2H-MoS ₂ /Activated Carbon Fiber Cloth for Solar Steam Generation. ACS Applied Materials & Interfaces, 2022, 14, 29788-29796.	4.0	18
106	Iron silicide-catalyzed growth of single-walled carbon nanotubes with a narrow diameter distribution. Carbon, 2019, 149, 139-143.	5.4	17
107	Realizable recycling of coal fly ash from solid waste for the fabrication of porous Al ₂ TiO ₅ â€Mullite composite ceramic. International Journal of Applied Ceramic Technology, 2019, 16, 50-58.	1.1	16
108	Enhanced acetone sensing properties of hollow SnO2 fibers using poplar catkins as a bio-template. Powder Technology, 2019, 344, 183-189.	2.1	16

#	Article	IF	CITATIONS
109	Fabrication of Three-Dimensional Porous NiO/Amorphous Ni(OH) ₂ Composites for Supercapacitors. Energy & Fuels, 2020, 34, 16783-16790.	2.5	16
110	A novel semi-metallic 1T′-MoReS3 co-catalyst. Chemical Engineering Journal, 2021, 425, 130525.	6.6	16
111	Stability, microstructure and mechanical properties of (Al,Fe) ₂ TiO ₅ porous ceramic reinforced by in-situ mullite. Journal of the Ceramic Society of Japan, 2015, 123, 156-159.	0.5	15
112	Semiâ€metal <scp>1T</scp> ′ phase <scp>MoS₂</scp> nanosheets for promoted electrocatalytic nitrogen reduction. EcoMat, 2021, 3, e12122.	6.8	15
113	Synthesis and characterization of Au-loaded SnO2 mesoporous spheres by spray drying and their gas sensing property. Materials Science in Semiconductor Processing, 2020, 105, 104710.	1.9	14
114	Synthesis of ZnO Hollow Microspheres and Analysis of Their Gas Sensing Properties for n-Butanol. Crystals, 2020, 10, 1010.	1.0	14
115	Au modified single crystalline and polycrystalline composite tin oxide for enhanced n-butanol sensing performance. Powder Technology, 2018, 331, 270-275.	2.1	13
116	Chemical Assembly of Titania P25 on MoO ₃ Nanobelts with Enhanced UV and Visible Photocatalytic Activities. Science of Advanced Materials, 2016, 8, 2313-2321.	0.1	13
117	Phonon spectrum and thermodynamic properties of LaCoO 3 based on first-principles theory. Computational Materials Science, 2017, 136, 191-197.	1.4	12
118	Preparation of meso-porous SnO2 fibers with enhanced sensitivity for n-butanol. Ceramics International, 2018, 44, 4990-4995.	2.3	12
119	Structural evolution and electrochemical corrosion behavior of Al–Ti–O amorphous-nanocrystalline composite films deposited by magnetron sputtering. Thin Solid Films, 2019, 692, 137640.	0.8	12
120	Facile fabrication of hierarchical structure SnO2 coatings using bioactive yeast cell. Materials Letters, 2016, 172, 137-141.	1.3	11
121	Preparation of porous Al ₂ O ₃ ceramics by starch consolidation casting method. International Journal of Applied Ceramic Technology, 2018, 15, 1550-1558.	1.1	11
122	Designing a 1D/2D W18O49/rGO heterostructure and constructing a bilayer structure of light absorber for highly efficient steam generation. Powder Technology, 2020, 361, 817-826.	2.1	11
123	Anisotropy thermoelectric and mechanical property of polycrystalline SnSe prepared under different processes. Journal of Materials Science: Materials in Electronics, 2019, 30, 6403-6410.	1.1	10
124	Influence of Cr Content on the Microstructure and Electrochemical Corrosion in Plasma Cladding Ni-Cr Coatings. Metallurgical and Materials Transactions A: Physical Metallurgy and Materials Science, 2019, 50, 5410-5420.	1.1	9
125	Enhanced Thermoelectric Performance of SnSe with Trace Au Particles via Transport Channel Design. ACS Applied Energy Materials, 2019, 2, 2604-2610.	2.5	9
126	The evolution of multi and hierarchical carbides and their collaborative wear-resisting effects in CoCrNi/WC composite coatings via laser cladding. Materials Today Communications, 2022, 30, 103223.	0.9	9

 ¹²⁷ Iridium-catalyzed growth of single-walled carbon nanotubes with a bicentric diameter distribution. Materials Chemistry Frontiers, 2019, 3, 1882-1887. 	3.2	8
128 Corrosion Resistance and Anti-wear Properties: Ni–W–GO Nanocomposite Coating with Lamellar Structure. Transactions of the Indian Institute of Metals, 2020, 73, 713-724.	0.7	8
Preparation of hierarchical porous Al2TiO5–mullite ceramics by biological foaming and its microstructural characterization. Ceramics International, 2019, 45, 8049-8053.	2.3	7
The phase structure and electrochemical performance of xLi2MnO3·(1Ââ´´Âx)LiNi1/3Co1/3Mn1/3O2 during the synthesis and charge–discharge process. Applied Physics A: Materials Science and Processing, 2016, 122, 1.	1.1	6
Atomic force microscopy investigation of a step generation and bunching on the (100) facet of a 131 CH ₃ NH ₃ PbI ₃ crystal, grown from γâ€Butyrolactone. Crystal Research and Technology, 2017, 52, 1700021.	0.6	6
¹³² Solution of boundary heat transfer coefficients between hot stamping die and cooling water based on FEM and optimization method. Heat and Mass Transfer, 2016, 52, 805-817.	1.2	5
Phase structure and electrochemical performance control of 0.5Li2MnO3â‹0.5LiNi1/3Co1/3Mn1/3O2 based on the concentration adjustment in a molten salt synthesis system. Journal of Applied Electrochemistry, 2017, 47, 691-698.	1.5	5
Microstructural characteristics of TiB ₂ –TiC–NiAl composite coatings via Plasma Cladding Process. Surface Engineering, 2019, 35, 997-1002.	1.1	5
An insight into the effects of transition metals on the thermal expansion of complex perovskite compounds: an experimental and density functional theory investigation. Physical Chemistry Chemical Physics, 2018, 20, 17781-17789.	1.3	4
 Investigation of single crystal growth of GaPO4 by the flux method. Crystallography Reports, 2013, 58, 195-197. 	0.1	2
¹³⁷ Conversion reaction mechanisms of cubic bismuth phosphate Bi13.1POδ as cathode in lithium-ion batteries. Journal of Materials Science, 2016, 51, 7598-7606.	1.7	2
Synthesis and characterization of coaxial SnO2–SiO x core–shell nanorods. Applied Physics A: Materials Science and Processing, 2016, 122, 1.	1.1	2
Mono-crystalline SnTe with micro-octahedroncharacteristic: One-pot facile synthesis and comprehensive crystallographic evidence. International Journal of Materials Research, 2019, 110, 460-465.	0.1	Ο
Effects of Solidification Rates on Microstructure Refinement and Elemental Distribution of 140 Ti44Al6Nb1.0Cr2.0V0.1B0.15Y Alloy by Rapid Solidification. Advanced Engineering Materials, 2021, 23, 2000809.	1.6	0
Multiscale Modelling and Characterization of Mechanical Properties in Heat-Resistant Alloys. Crystals, 2022, 12, 105.	1.0	0